Edinburgh Research Explorer

Momentum-map-imaging photoelectron spectroscopy of fullerenes with femtosecond laser pulses

Momentum-map-imaging photoelectron spectroscopy of fullerenes with femtosecond laser pulses

M. Kjellberg,[1] O. Johansson,[1,2] F. Jonsson,[1] A. V. Bulgakov,[1,*] C. Bordas,[3] E. E. B. Campbell,[1,2] and K. Hansen[1]

[1]*Department of Physics, University of Gothenburg, 41296 Gothenburg, Sweden*
[2]*School of Chemistry, University of Edinburgh, Edinburgh EH9 3JJ, United Kingdom*
[3]*Université de Lyon, CNRS, UMR5579, LASIM, F-69622 Lyon, France*

Photoelectron spectra of C_{60} and C_{70}, ionized with ultrashort laser pulses, are measured with a momentum-map-imaging electron spectrometer. Above the photon energy, 1.6 eV, the spectra are essentially structureless and well described by Boltzmann distributions, with temperatures on the order of 10^4 K. This result is similar to previous results for C_{60} using a time-of-flight electron spectrometer, which are confirmed in this study. Comparisons of electron energy distributions recorded for identical laser intensities but for different pulse durations demonstrate unambiguously that a significant fraction of the electrons are emitted in quasithermal processes and results argue strongly against a field ionization or direct multiphoton ionization mechanism. For electron energies above the photon energy, which account for about half the intensity, the whole signal is consistent with this quasithermal emission.

I. INTRODUCTION

With the increasing availability of short-pulse lasers, our understanding of the mechanisms of ionization of gas phase species continues to develop. The ionization of atoms has been studied in great detail for a long time and several mechanisms have been identified, among these above-threshold ionization (ATI) and, at higher intensities, field ionization [1,2]. These ionization mechanisms are also observed for molecules, for example in the ATI for C_{60} [3]. However, for molecules, another ionization mechanism can be active: transient hot electron ionization [3–5]. This process is thermal by nature, proceeding from a hot electron subsystem in quasiequilibrium before it equilibrates with the vibrational degrees of freedom. It has close analogies to thermionic emission, which describes thermal electron emission from a system in complete thermal equilibrium [6,7]. Transient hot electron emission, however, is characterized by a relatively cold vibrational system. The main observable differences between the two types of thermal emission are related to the finite electron-vibrational equilibration time, which implies that the transient hot electron emission requires subpicosecond excitation, and to the low heat capacity of the electronic system relative to the vibrational system. For times short compared to the electronic-vibrational relaxation time, the electronic system can be heated to temperatures well above those at which a fully equilibrated molecule would rapidly dissociate. For C_{60}, the excitation energy was estimated to couple from the electronic system to vibrations with a time constant that was fitted from experimental Boltzmann-like electron kinetic energy spectra using a relatively simple thermal emission model and found to be 240 fs [5].

A Boltzmann-like electron kinetic energy spectrum is in itself not proof of a thermal ionization mechanism. Other ionization mechanisms may produce similarly structureless photoelectron spectra. We have shown previously for C_{60} that

a thermal ionization mechanism, however, is consistent with a range of experimental data such as ion yields and relative charge-state intensities, as well as the photoelectron spectra, for excitation with laser pulses of duration on the order of a few hundred femtoseconds [5,8]. The thermal emission model was originally introduced to explain Penning ionization results with C_{60} [4], i.e., situations where strong field ionization is obviously excluded. For pulses shorter than 100 fs, and pulse energies similar to the ones used in the present work, direct (prompt) ionization mechanisms dominate, such as ATI or field ionization, as seen in the shortest pulse electron spectra in [3] or from the pump-probe ion yields in [9]. The latter reference unfortunately does not report electron spectra.

A thermal electron emission similar to the one proposed for fullerenes has also been invoked to explain the photoelectron spectra obtained from sodium clusters [10,11] as well as the ionization of rare gas clusters with photons with energies high above the ionization threshold [12]. The description of the electrons as transiently hot is similar to the so-called two-temperature model used in solid state physics to describe the behavior of the valence electrons when rapidly excited by a short laser pulse, for example, similar to the present experiments. Interestingly, a very similar mechanism invoking the existence of a dense spectrum of chaotic multiply excited states has been suggested to explain the exceptionally high electron recombination rates of many-electron multiply charged ions [13].

Although the transient hot electron ionization mechanism is consistent with many experimental observations [5], a number of fundamental questions concerning the applicability and generality of the mechanism remain unanswered. A linear time-of-flight photoelectron spectrometer, as was used for the earlier studies, has limited detection efficiency for low-energy electrons and is also unsuited to the accurate determination of photoelectron angular distributions.

A momentum-map-imaging spectrometer, on the other hand, allows the simultaneous detection of photoelectron kinetic energies and angular distributions and is thus ideally suited to explore the fundamental ionization mechanisms of molecules and clusters. In this paper, we report the first

―――――――
*Permanent address: Russian Academy of Science, Institute of Thermophysics SB RAS, Prospect Lavrentyev 1, 630090 Novosibirsk, Russia.

results obtained from a combined momentum-map-imaging photoelectron spectrometer and time-of-flight mass spectrometer designed to investigate the time-dependent ionization processes in large molecular systems. The results obtained for C_{60} are consistent with the earlier time-of-flight photoelectron spectra for similar laser excitation conditions, and the results of several experiments that have been performed on C_{70} are given. Most important, by comparing emission characteristics for the same laser fluences but different pulse durations and, hence, laser intensities, we provide further evidence for the thermal nature of the electron emission which occurs prior to energy equilibration with vibrational degrees of freedom.

II. EXPERIMENTAL

The fullerene source is a resistively heated effusive sublimation source. The commercial fullerene powder, with a purity of 99.5% for C_{60} and 98% for C_{70}, is heated in an oven to 450°C and the fullerene vapor effuses to the center of the extraction zone of the electron spectrometer, where the interaction with the laser field takes place.

The electron spectrometer is based on the momentum map imaging technique [14,15]. The design of our spectrometer is similar to the one described in [16], although some changes were made to the original design for reasons of compatibility with existing equipment. A schematic picture is shown in Fig. 1.
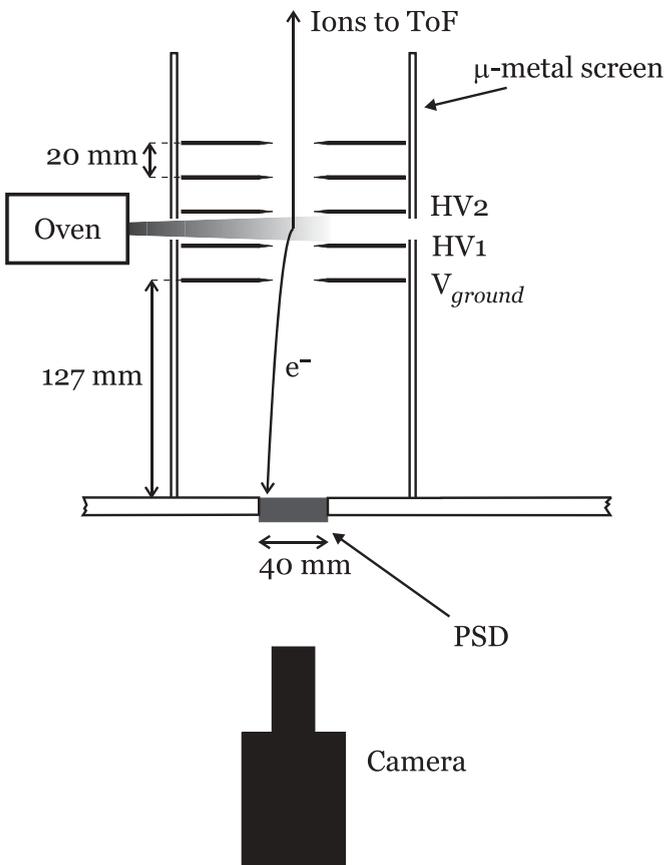

FIG. 1. A schematic picture of the electron spectrometer. See main text for more details.

To eliminate external magnetic fields, the entire spectrometer is surrounded by a 1.57 mm thick μ-metal cylinder from Amuneal Manufacturing Corporation. The cylinder is 260 mm long, has an inner radius of 135 mm, and has open ends. Four apertures in the cylinder allow entry and exit of the molecular beam and the laser beam in a perpendicular configuration. The apertures are 12×22 mm^2, with the short dimension along the cylinder axis. The μ-metal cylinder is fixed to the grounded exit electrode on the ion side with four M3 screws, and the cylinder is positioned in a 3 mm deep groove in the flange where the position sensitive detector (PSD) is mounted, which gives further support.

The photoelectrons produced in the laser–molecule interaction are extracted from the interaction region and projected onto the PSD by two electric fields. The electric fields, which are typically of several hundred V/cm, are applied between three electrodes, HV2, HV1, and V_{ground}, which are separated by 20 mm, center-to-center. The inner diameter of the electrodes is 24 mm and the thickness of the electrodes is tapered radially with an angle of 14° to an outer thickness of 2 mm and a rounded edge with a radius of ca. 0.05 mm. The electrodes are stacked on four rods of 5 mm diameter and the whole electrode package is mounted on the flange with four rods of 8 mm diameter. Between V_{ground} and the PSD, a 120 mm long field-free region is used to separate the photoelectrons in space according to their momenta. With typical potentials of -2300 and -1500 V for HV2 and HV1, respectively, the maximum detectable kinetic energy, corresponding to detection at the edge of the detector, is 11 eV. No meshes are mounted between the laser–molecular beam interaction region and the PSD, although one, with a transmission of 90%, is present at the exit electrode of the ion mass spectrometer section.

For a certain ratio of the two electric fields, all electrons with the same component of momentum parallel to the detector plane will, to a good approximation, hit the same place on the PSD regardless of where they were produced in the interaction region [15]. For an illustration of this focusing behavior, see Fig. 2. The condition for this momentum mapping was found by visual optimization of the resolution of the circular ATI rings in the momentum map of photoelectrons from xenon atoms, shown in Fig. 2.

The PSD consists of a commercial assembly of dual, chevron style, micro channel plates (MCP) and a phosphor screen (Burle industries GmbH, APD 3040 FM 12/10 I P20 PN 30019). The phosphor screen has a 40 mm effective diameter and a 0.2 ms "bleed off" time. Typically a voltage of 1.5-1.6 kV is applied over the MCPs. The impacting photoelectrons are amplified in the MCP and at the back end of the MCP the electrons are further accelerated up to 4.5–5.0 kV and ejected toward the phosphor screen. The bunches of electrons hitting the phosphor screen create flashes of fluorescence light, that can be seen on the atmosphere side of the screen. A Firewire connected CCD camera (Allied Vision Technologies, Dolphin 201B, 1628×1236 pixels) records images of the phosphor screen. The images are sent to a computer where they are accumulated with a Labview routine. The camera shutter is open for 80 milliseconds, corresponding to 80 laser pulses of the 1 kHz laser. Every spectrum presented in this paper is a sum of 1000–5000 images minus the same number of
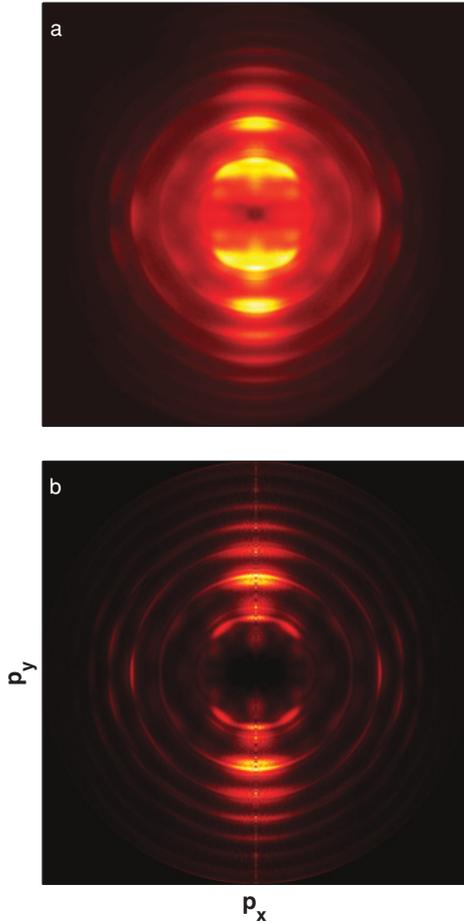
FIG. 2. (Color online) (a) Raw data, momentum map image of xenon after femtosecond laser ionization. (b) Inverted image, representing the $p_z = 0$ slice of the original three-dimensional distribution. The whole three-dimensional distribution can be reconstructed using the cylindrical symmetry, caused by the laser polarization. The laser peak intensity is 6.4×10^{13} W/cm^2. The laser polarization is in the y direction, parallel to the detector; p_x and p_y correspond to the momentum of the photoelectrons. Colors (online only) are saturated for display purposes.

images where only the background is recorded, i.e. without the laser but otherwise identical conditions. Because the laser polarization is parallel to the PSD, the original 3D-distribution of photoelectrons can be reconstructed via an inverse Abel transform. The raw data image is first symmetrized as the average of the four quadrants defined by the laser's polarization and propagation vectors and then inverted according to the algorithm given in [17]. The inverted momentum map of photoelectrons from xenon is shown in Fig. 2(b). The noise in the central column of the inverted image in Fig. 2 is due to accumulated numerical noise generated in the inversion algorithm.

The momentum of the photoelectrons is linear on the scale of the raw data image. The energies of the ATI rings in the xenon spectrum in Fig. 2 are known and are used for energy calibration. In Fig. 3, the angle-integrated kinetic energy spectrum of xenon is shown in pixel units. The ATI peaks are separated by the photon energy of the laser, $h\nu = 1.59$ eV.
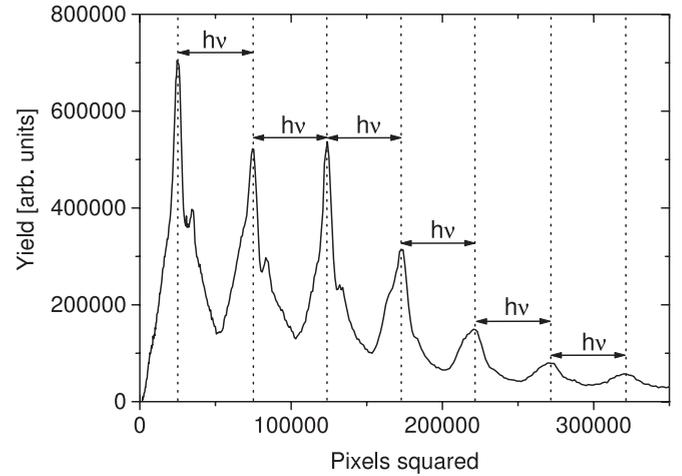

FIG. 3. Energy calibration of the electron spectrometer using the ATI peaks of ionized xenon atoms. The arrows have a length of 1.59 eV, which is the centroid photon energy of the fs laser and the distance between the ATI peaks.

Six identical arrows of length $h\nu$ are inserted in the spectrum at the location of the ATI peaks, illustrating the conversion factor from pixels squared to eV.

Photoions are detected in the time-of-flight mass spectrometer part of the instrument by changing the polarity of the acceleration electrodes. The mass spectrometer can be used in linear mode or as a reflectron. The change from photoelectron to photoion detection takes a few minutes, which ensures that electron spectra and mass spectra are recorded under similar conditions.

A. Laser characteristics

The fs laser that has been used is a commercial titanium:sapphire laser (Clark-MXR CPA-2001). The fundamental wavelength is 780 nm (1.59 eV) and the beam is of Gaussian shape. The maximum output power is up to 900 mW at a repetition rate of 1 kHz. The pulse duration at full width at half maximum (FWHM) is 150 ± 5 fs and was measured by a commercial autocorrelator (APE Pulse Check).

To attenuate the laser beam, neutral density filters, beam splitters, and a combination of a $\lambda/2$ wave plate and a Glan laser calcite polarizer were used. The Glan laser polarizer was also used to fix the laser polarization parallel to the PSD. The laser beam was focused into the center of the electron spectrometer by a lens of 30 cm focal distance.

The laser power was measured with a Coherent Fieldmaster power meter. The laser intensity was calibrated by measurements of the yield of xenon ions. The intensities given here all refer to the center of the laser beam and a calibration relative to the intensities given in [18]. In the pulse-duration-dependence measurements the 150-fs pulses were stretched up to 1.53 ps by detuning the compressor after amplification.

For the reference electron spectroscopy measurements of ns laser ionization, a commercial N$_2$ laser (Laser Science, Inc., VSL337ND-S) was used. The photon energy is 3.68 eV and the pulse duration is specified to be shorter than 4 ns.

III. RESULTS AND INTERPRETATION

In Figs. 4 and 5, raw data images and inverted images for C_{60} and C_{70} are shown for a laser intensity of 1.23×10^{13} W/cm^2, corresponding to a laser fluence of 1.84 J/cm^2. (The uncertainties in the fluence in the present study are essentially only systematic.) As discussed later, the laser fluence is the most appropriate parameter in this study; for that reason, we typically state the laser fluence rather than the laser intensity. The 2π angle-integrated electron spectra of C_{60} and C_{70} are shown in Figs. 6 and 7 for a number of different fs-laser fluences, ranging from 1.13 J/cm^2 for the bottom curve to 2.19 J/cm^2 for the top curve (all for a pulse duration of 150 ± 5 fs). The corresponding laser intensities are all within the multiphoton ionization regime, as indicated by the Keldysh parameter that has values in the range 2–3. The Keldysh parameter, γ, is defined as

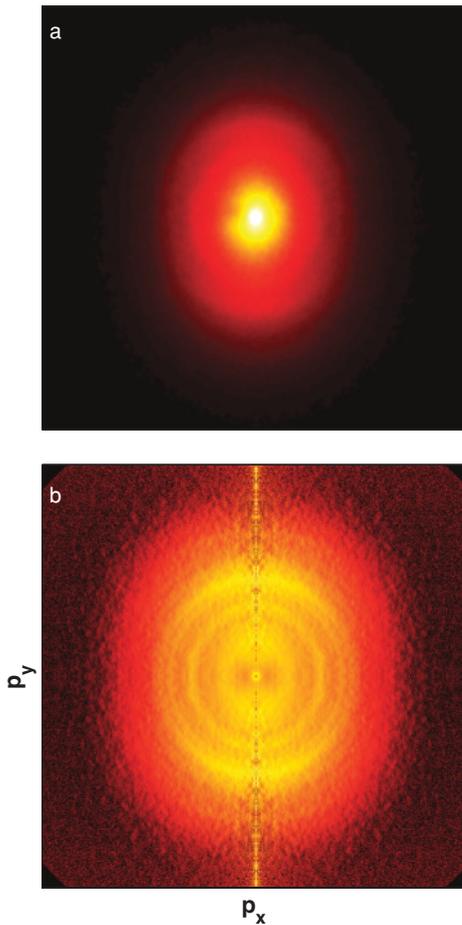$$\gamma = \sqrt{\frac{\Phi}{2U_p}}, \quad U_p = \frac{e^2 E_0^2}{4m\omega^2}, \tag{1}$$

FIG. 4. (Color online) C_{60} momentum map, at laser fluence 1.84 J/cm^2: (a) raw image, linear scale; (b) inverted image, logarithmic scale. The intense central rings are associated with Rydberg states [19]. The laser polarization is in the y direction, parallel to the detector; p_x and p_y correspond the momentum of the photoelectrons. Colors (online only) are saturated for display purposes.
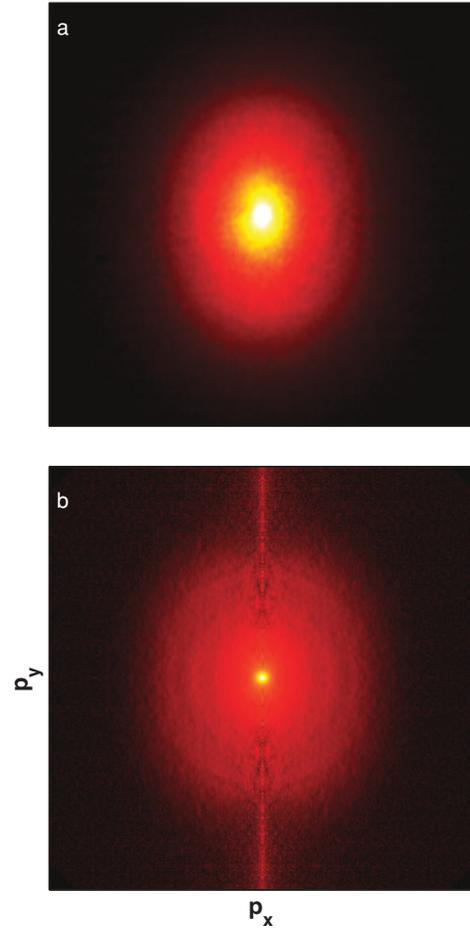

FIG. 5. (Color online) C_{70} momentum map. All other data are the same as in Fig. 4.

where Φ is the ionization potential; U_p is the ponderomotive potential; e and m are the electron charge and mass, respectively; E_0 is the electric field amplitude; and ω is the angular frequency of the light [20]. Photoelectron spectra after excitation with the ns laser are also included to demonstrate the difference in the photoelectron spectra for fs and ns excitation.

The mass spectra for a laser fluence of 1.13 J/cm^2 are shown in Figs. 6 and 7. For fluences greater than 2.19 J/cm^2, which is the highest used in this study, more intense fragmentation sets in and measurements at these fluences are therefore not considered here. No correction for the detection efficiency has been made. The low m/q species (small fragments, doubly ionized species) are therefore disproportionately strongly represented.

Compared to the case of atomic xenon, where the spectrum is composed of discrete ATI peaks, the photoelectron spectra of the fullerenes are seen to be a superposition of a structureless exponentially decreasing component, previously interpreted for C_{60} (correctly, we believe), as being due to thermal electron emission from hot electrons [5], and structure due to the direct, single-photon ionization of Rydberg states [3]. (Individual Rydberg peaks are unresolved for the current laser excitation conditions.) At high intensities a weak signal corresponding to the second ATI peak is present in the spectrum for C_{60}
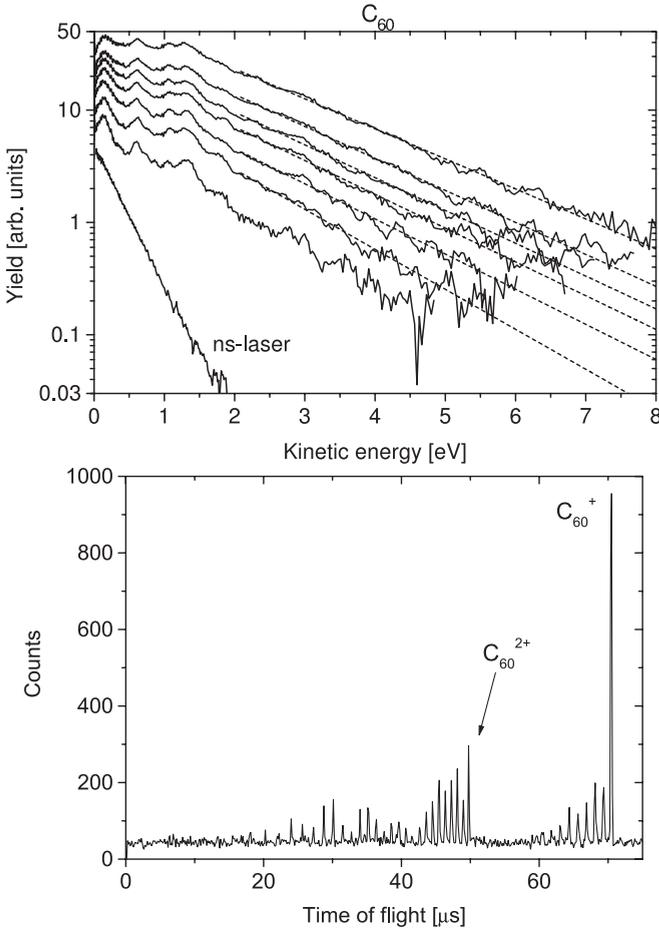
FIG. 6. C_{60} electron and mass spectra. From top to bottom, the fs-pulse fluences are 2.19, 1.84, 1.70, 1.56, 1.42, 1.27, and 1.13 J/cm^2 in the electron spectra. The spectra are cut at the noise level. The bottom curve corresponds to ns excitation. The mass spectrum corresponds to the fs-laser fluence 1.13 J/cm^2.

(Fig. 6). The relative intensities of the electron spectra below the photon energy and higher are comparable, in the spectra of both Fig. 6 and Fig. 7.

The inverse of the slope of the structureless component in a semilogarithmic plot can be interpreted as the apparent electronic temperature, T_a [5]:

$$P(\epsilon) \propto \exp(-\epsilon/T_a), \qquad (2)$$

where ϵ is the electron kinetic energy. We have set Boltzmann's constant equal to unity. This choice of units is particularly convenient here because temperatures are usually in the range of 1 eV. It is, in a rigorous sense, incorrect to describe the spectra as Boltzmann distributions and to use a simple exponential fit to determine the temperature, because the system is best described as microcanonical (i.e., it does not have a rigorously defined temperature). For a general discussion of the concept of temperature in a microcanonical system, see [21,22]. The main approximation made in fitting a temperature to a spectrum is the neglect of factors such as photon absorption statistics and the time dependence of the excitation energy. As shown numerically [5], these effects only introduce minor differences between the fitted temperature and those expected from the molecules ionized at the peak
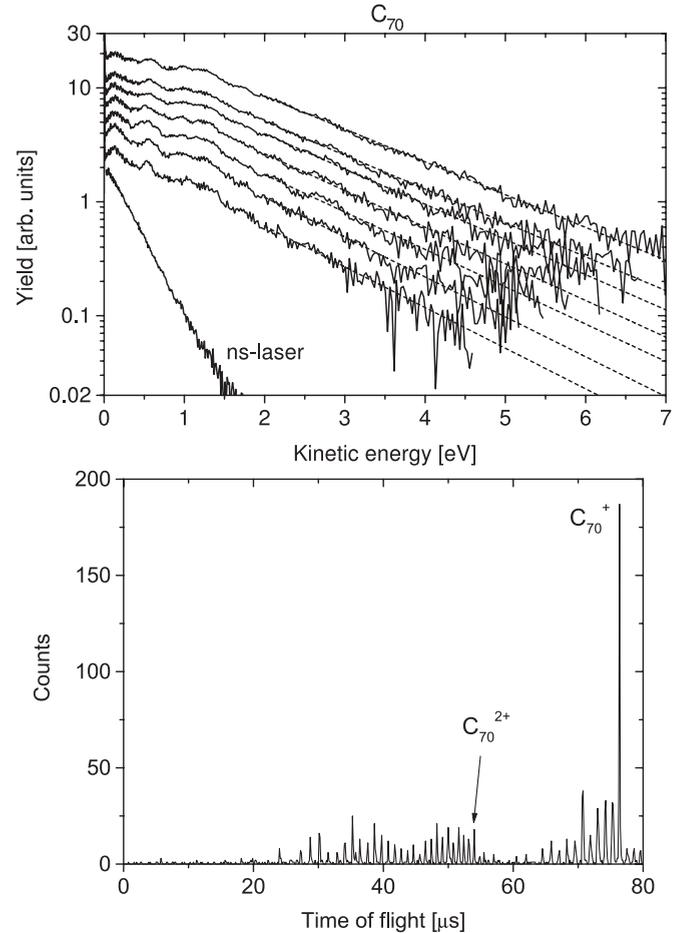
FIG. 7. C_{70} electron and mass spectra. The laser fluences and durations are identical to those of Fig. 6.

power in the center of the laser beam. The apparent electronic temperature, T_a, therefore serves as a good parameter for the comparison of different types of distributions.

As can be seen from Figs. 4 and 5, the angular distribution of the structureless "thermal" electron signal is slightly elongated along the laser polarization direction, and this distortion becomes most pronounced for the highest laser intensities. The observed asymmetry is interpreted as an effect of the electric field experienced by the electrons that are thermally emitted during the laser pulse. The time scale for the quasithermal electron emission is of the same order of magnitude as the duration of the laser pulse [5], and the momenta of the ejected electrons are thus influenced by the laser field. The asymmetry is the subject of a separate publication [23]. For the present purpose, we just note that the asymmetry is observed to cause only minor modifications of the exponential decrease of the angle-integrated spectrum with respect to energy, and the angle-integrated data are used in the following.

A. Fluence dependence

The electronic temperatures, T_a, obtained from the fits are shown versus laser fluence in Fig. 8. The data compare rather well with the temperatures of C_{60} from [5], obtained with nominally identical laser parameters in a similar experimental setup but using a time-of-flight electron spectrometer
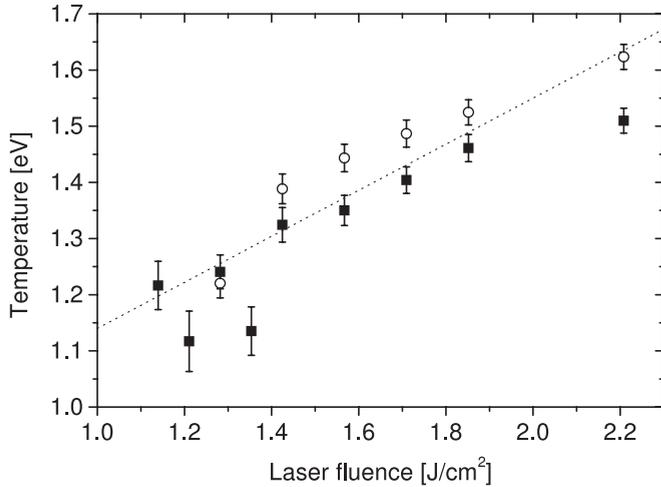
FIG. 8. The apparent electronic temperature as a function of laser fluence. Squares, C_{70}; circles, C_{60}. The dotted line is the fit to the temperatures vs laser fluence for C_{60} from [5]. The laser fluence has an overall systematic uncertainty of 10%, which is not included in the error bars.

instead of the imaging spectrometer of the present work. The literature results are represented by the dotted line. The difference between the present C_{60} data and those of [5] corresponds to a difference in laser fluence of around 5%, which is within the systematic experimental uncertainty. The electronic temperatures extracted for C_{70} range from 13,200 K (1.14 eV) to 17,500 K (1.51 eV) for increasing laser fluence in the range 1.1–2.2 J/cm² (i.e., slightly lower than those of C_{60}). As discussed in the introduction and in our previous work on C_{60} [3,5], these extremely high temperatures indicate that the ionization dynamics is different from the thermionic electron emission after ns excitation, where much lower electron temperatures are observed. The C_{60} ns spectrum in Fig. 6, for example, corresponds to a temperature of 3800 K (0.33 eV). Even with high-intensity ns lasers, electronic temperatures are rarely above 4000 K, and temperatures above 5000 K are never observed in these processes due to the strong dominance of neutral fragmentation for very highly excited fullerenes [24]. In contrast, the ionization with fs laser pulses (Fig. 8) shows an approximately linear increase of temperature with the fluence in the investigated range, far above the ns laser pulse value of 0.33 eV.

The very similar fluence dependence of the temperatures of C_{60} and C_{70} is evidence of similar photon absorption cross sections for these two species. At high excitation energy, the electronic level density of both species can be expected to be reasonably well approximated by the Fermi gas values, for which the caloric curve has the form

$$T \propto (E E_F / N)^{1/2}, \qquad (3)$$

where N is the number of valence electrons; E_F is the Fermi energy, which can be defined here as the kinetic energy of the highest occupied molecular level in the ground state; E is the excitation energy; and T is the temperature. This expression holds for both canonical and microcanonical ensembles to a reasonable extent, in the latter case approximately, provided the temperature is defined as the microcanonical temperature

(as mentioned earlier in connection with the discussion of the effective emission temperature). The typical electronic energy of the molecules that emit an electron is given by

$$E \propto \sigma F, \qquad (4)$$

where σ is the average one-photon absorption cross section and F is the laser fluence. Combining these two expressions gives

$$T \propto (\sigma/N)^{1/2} \rightarrow \frac{\sigma_{70}}{\sigma_{60}} = \frac{70}{60}(T_{70}/T_{60})^2 \qquad (5)$$

for the temperatures extracted from identical fluences and assuming the same E_F for C_{60} and C_{70}. The observed temperature differences for C_{60} and C_{70} are 5% on average. This ratio then yields the ratio of average photon absorption cross sections to be $\sigma_{70}/\sigma_{60} \approx 1.06$. This estimate is fairly robust with respect to the caloric curve in Eq. (3). One may expect modifications of this value due to the finite pulse duration, but we do not expect that to change the ratio significantly.

B. Pulse-duration dependence

The pulse-duration variation of the electron emission temperature was measured for C_{70}. The pulse duration was changed by detuning the compressor stage of the laser and maintaining the laser fluence at 1.84 J/cm². The autocorrelation curves for the stretched pulses were still close to Gaussian with a correspondingly larger FWHM. The electron emission mechanism is intrinsically delayed and the measured stretched pulse temperatures allow a test of the emission mechanism. The main difference between ionization occurring in a direct field ionization or multiphoton process and in a quasithermal mechanism is that the former is sensitive to the field and the latter to the total fluence. In other words, a field-ionization mechanism is sensitive only to the instantaneous electric field and does not depend on the fluence or the pulse duration. Therefore, for field ionization the measured apparent temperatures should be identical for short and long pulses if the pulses have identical peak intensities. The "apparent temperature" refers in this analysis to a parametrization of the shapes of the electron spectra and not necessarily to the physical mechanism generating these spectra. For a delayed, thermal ionization of the type we suggest, the apparent temperature should be higher for longer pulses and identical peak intensity. This makes the question susceptible to an experimental test without any need to rely on modeling of the specific processes. The data are shown in Fig. 9. Starting from the right-most data point, which corresponds to a pulse duration of 150 fs and a peak intensity of 12.3×10^{12} W/cm², the laser intensity was reduced either by lowering the laser fluence while keeping the pulse duration fixed (crosses), or by keeping the laser fluence fixed and stretching the pulse in time (squares). As can be seen, the first scenario leads to a considerably steeper reduction of the electronic temperature, which is also what would be expected from a thermal ionization process where the laser fluence is expected to be the relevant parameter.

The data shown in Fig. 9 allow a more detailed comparison between spectra for the purpose of assessing the thermal nature of the electron emission process.
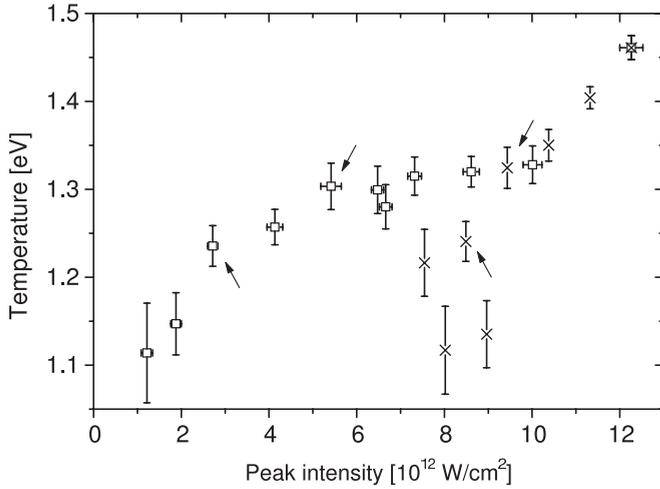
FIG. 9. Electronic temperature of C_{70} photoelectrons as a function of peak intensity. Crosses correspond to a fixed pulse duration, 150 fs, and varying pulse energy. Open squares correspond to a fixed laser fluence, 1.84 J/cm^2, and varying pulse duration from 150 up to 1528 fs. The uncertainties in temperature are those of the fitting procedure, and those of the intensities are mainly from the autocorrelation function. The systematic uncertainty in the absolute fluence calibration is irrelevant for the comparison here and is not included. The arrows indicate the spectra used in Fig. 10.

Figure 10 shows electron energy distributions for stretched [Fig. 10(a), 680 fs; Fig. 10(b), 340 fs] and short (150-fs) pulses with different pulse energies but selected to have identical apparent electron temperatures. The comparison shows that for electron kinetic energies below the photon energy, 1.59 eV, where structure from single-photon ionization of Rydberg states dominates the spectra, the intensities are very similar once the thermal parts of the distributions, greater than 1.59 eV, are scaled to give identical values. This may indicate a
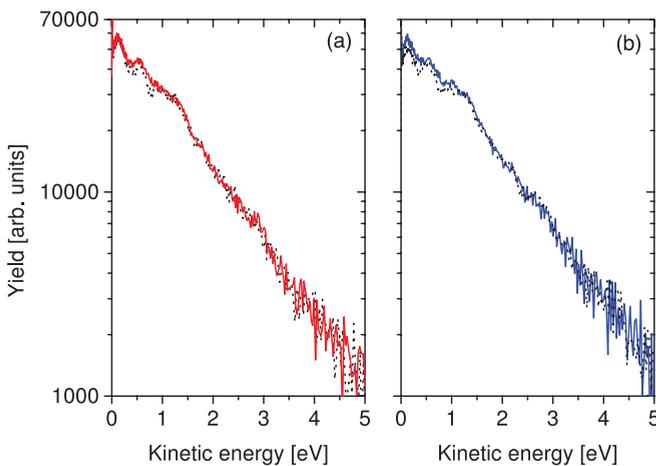

FIG. 10. (Color) Photoelectron spectra from C_{70} for stretched and short pulses with approximately the same electron temperatures. (a) Black, dotted, curve: 150 fs, 1.27 J/cm^2, $T_a = 1.24$ eV; red, full, curve: 680 fs, 1.84 J/cm^2, $T_a = 1.24$ eV. (b) Black, dotted, curve: 150 fs, 1.42 J/cm^2, $T_a = 1.32$ eV; blue, full, curve: 340 fs, 1.84 J/cm^2, $T_a = 1.30$ eV. The spectra are scaled to give identical values of the thermal parts above the photon energy, 1.59 eV.
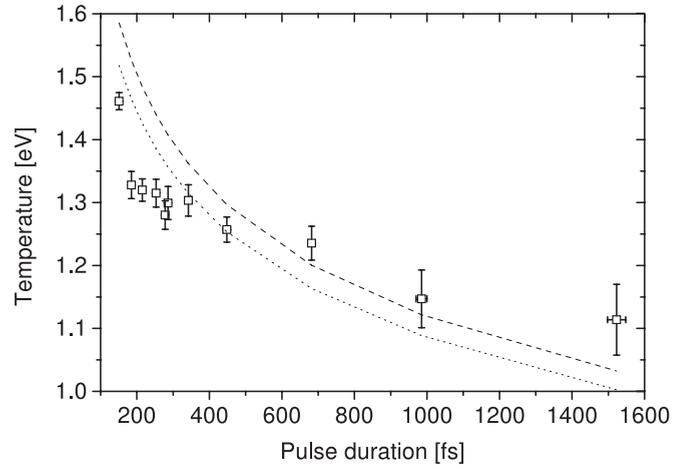

FIG. 11. The electronic temperatures for different pulse duration at fixed laser fluence (1.84 J/cm^2) for C_{70}. The experimental data are the stretched pulse data from Fig. 9. The simulated curves are the average electronic temperature of the ion at the time of emission, calculated for two different electron-vibrational coupling times. The dashed curve corresponds to a coupling time of 400 fs and a total of 190 photons (300 eV) absorbed in the pulse. The dotted line corresponds to 600 fs and 100 photons (160 eV). The lines are not fit curves and several sets of parameters give similar curves.

similar population mechanism for the thermal electrons and the excited Rydberg states and is the subject of ongoing investigations. It also simplifies a comparison of ion yields that are heavily influenced by the low-energy part of the spectrum, and therefore potentially unrelated to electron temperatures, to be used as proxies for the more demanding measurements of the whole electron kinetic energy distributions. For the data shown, the integrated electron yields differ by 4% and 5% in Figs. 10(a) and 10(b), respectively.

The data in Fig. 9 are plotted as a function of pulse duration in Fig. 11 and show that the apparent electronic temperature decreases for a longer pulse duration. Two factors contribute to this drop. One is the dissipation of the electronic excitations into the molecular vibrations, which causes a longer pulse with the same energy to reach a lower maximum temperature and more generally gives a lower temperature for otherwise identical conditions. The other effect that can lower the measured temperature for a stretched pulse is that the electrons may be emitted before the electronic excitation energy content of the molecule at time t, $E(t)$, peaks. The excitation energy at which this happens is generally lower for longer pulses. These two effects are difficult to disentangle analytically and we have therefore simulated the data in Fig. 9 numerically.

The simulation proceeds as follows. The surviving fraction of neutral molecules is

$$P(t) = \exp\left[-\int_{-\infty}^{t} k(E(t'))dt' \right]. \quad (6)$$

The ionization yield is then

$$\frac{dY(t)}{dt} = -\frac{dP(t)}{dt} = k \exp\left(-\int_{-\infty}^{t} kdt' \right), \quad (7)$$

where the energy arguments have been suppressed for ease of notation. The expression for the rate constant is

approximately

$$k = \omega e^{-\Phi/T}, \tag{8}$$

where T is the emission temperature, which is close to the mean of the parent and product temperature, and related to the measured, apparent temperature by $T_a \approx T - \Phi/2C_v$. The ionization energy is $\Phi = 7.6$ eV. The heat capacity is that of a three-dimensional Fermi gas,

$$C_v = \frac{\pi^2 N T}{2 E_F}, \tag{9}$$

where N is the number of electrons ($N = 280$), and $E_F = 30$ eV is assumed to be similar to the value for C_{60} [25]. Using the temperature of 1.3 eV to calculate the weakly energy-dependent frequency factor, we get $\omega = 9 \times 10^{15}$ s^{-1}. In the simulations a slightly smaller value was used: $\omega = 5 \times 10^{15}$ s^{-1}.

The numerical estimates were made as an integration over the pulse duration and by sampling the average temperature, for one electron emission only. Apart from the pulse duration, the number of absorbed photons and the coupling time to vibrations were varied in the simulations. The dependence on the absorbed energy was weak apart from the low-energy end, where 10–20 photons were absorbed during the whole pulse, and it reproduced the experimentally observed data reasonably well, irrespective of the precise value of the coupling time. The coupling time was varied between 100 fs and 1 ps in steps of 100 fs. The dependence on this parameter was very weak.

After comparing the electronic temperature for varying pulse duration for C_{60} reported in [5] and for C_{70} in this study, it seems that the drop in temperature with increased pulse duration occurs somewhat more quickly for C_{60}.

IV. CONCLUSIONS

We have measured photoelectron spectra of C_{70} and C_{60} after 780 nm ultrashort-pulse laser excitation with a momentum-map-imaging electron spectrometer. The performance of the spectrometer was tested with measurements of the spectra of C_{60} and atomic xenon, which were found to be in good agreement with results reported in the literature [5,26].

The spectra of C_{70} and C_{60} are very similar to each other and have a strong thermal component. Extremely high electronic temperatures, up to 1.51 eV (17,500 K) for C_{70} and 1.62 eV (18,800 K) for C_{60}, are observed. These electron energy distributions are demonstrated to result from statistical electron emission from a highly excited electronic subsystem where the nuclear vibrations remain cold. The responses of the two different fullerene molecules to the laser are very similar and support interpretations of the data that do *not* rely on specific features in the excitation spectra of the molecules. The photoelectron spectra for varying pulse durations are quantitatively consistent with an explanation in terms of a transient hot electron gas and inconsistent with a direct multiphoton or field-ionization scenario.

[1] J. H. Eberly, J. Javanainen, and K. Rzążewski, Phys. Rep. **204**, 331 (1991).

[2] M. Protopapas, C. H. Keitel, and P. L. Knight, Rep. Prog. Phys. **60**, 389 (1997).

[3] E. E. B. Campbell, K. Hansen, K. Hoffmann, G. Korn, M. Tchaplyguine, M. Wittmann, and I. V. Hertel, Phys. Rev. Lett. **84**, 2128 (2000).

[4] J. M. Weber, K. Hansen, M.-W. Ruf, and H. Hotop, Chem. Phys. **239**, 271 (1998).

[5] K. Hansen, K. Hoffmann, and E. E. B. Campbell, J. Chem. Phys. **119**, 2513 (2003).

[6] E. E. B. Campbell, G. Ulmer, and I. V. Hertel, Phys. Rev. Lett. **67**, 1986 (1991).

[7] T. Leisner, K. Athanassenas, O. Echt, O. Kandler, D. Kreisle, and E. Recknagel, Z. Phys. D **20**, 127 (1991).

[8] A. Lassesson, K. Hansen, M. Jönsson, A. Gromov, E. E. B. Campbell, M. Boyle, D. Pop, C. P. Schulz, I. V. Hertel, A. Taninaka, and H. Shinohara, Eur. Phys. J. D **34**, 205 (2005).

[9] I. Shchatsinin, T. Laarmann, G. Stibenz, G. Steinmeyer, A. Stalmashonak, N. Zhavoronkov, C. P. Schultz, and I. V. Hertel, J. Chem. Phys. **125**, 194320 (2006).

[10] R. Schlipper, R. Kusche, B. v. Issendorff, and H. Haberland, Appl. Phys. A **72**, 255 (2001).

[11] M. Maier, M. Astruc Hoffmann, and B. v. Issendorff, New J. Phys. **5**, 3 (2003).

[12] T. Laarmann, M. Rusek, H. Wabnitz, J. Schulz, A. R. B. de Castro, P. Gürtler, W. Laasch, and T. Möller, Phys. Rev. Lett. **95**, 063402 (2005).

[13] V. V. Flambaum, A. A. Gribakina, G. F. Gribakin, and C. Harabati, Phys. Rev. A **66**, 012713 (2002).

[14] H. Helm, N. Bjerre, M. J. Dyer, D. L. Huestis, and M. Saeed, Phys. Rev. Lett. **70**, 3221 (1993).

[15] A. T. J. B. Eppink and D. H. Parker, Rev. Sci. Instrum. **68**, 3477 (1997).

[16] B. Baguenard, J. B. Wills, F. Pagliarulo, F. Lépine, B. Climen, M. Barbaire, C. Clavier, M. A. Lebeault, and C. Bordas, Rev. Sci. Instrum. **75**, 324 (2004).

[17] C. Bordas, F. Paulig, H. Helm, and D. L. Huestis, Rev. Sci. Instrum. **67**, 2257 (1996).

[18] S. F. J. Larochelle, A. Talebpour, and S. L. Chin, J. Phys. B **31**, 1215 (1997).

[19] M. Boyle, K. Hoffmann, C. P. Schulz, I. V. Hertel, R. D. Levine, and E. E. B. Campbell, Phys. Rev. Lett. **87**, 273401 (2001).

[20] L. V. Keldysh, Sov. Phys. JETP **20**, 1307 (1965).

[21] C. E. Klots, Chem. Phys. Lett. **186**, 73 (1991).

[22] J. U. Andersen, E. Bonderup, and K. Hansen, J. Chem. Phys. **114**, 6518 (2001).

[23] M. Kjellberg *et al.* (to be published).

[24] F. Lépine, B. Climen, M. A. Lebeault, and C. Bordas, Eur. Phys. J. D **55**, 627 (2009).

[25] K. Hansen, in *AIP Conference Proceedings* (New York, 1998), Vol. 416.

[26] V. Schyja, T. Lang, and H. Helm, Phys. Rev. A **57**, 3692 (1998).